Journal of Polymer Research (2020) 27: 381
https://doi.org/10.1007/s10965-020-02356-2

ORIGINAL PAPER

# Electrospinning of antibacterial cellulose acetate/polyethylene glycol fiber with *in situ* reduced silver particles

**Sushmita Majumder[1] · Md Abdul Matin[2] · Ahmed Sharif[1] · M Tarik Arafat[3]**

Received: 26 May 2020 / Accepted: 17 November 2020 / Published online: 20 November 2020


## Abstract

A novel composition of antibacterial fiber mat, consisting of cellulose acetate (CA), polyethylene glycol (PEG) and silver particles (AgPs) was fabricated by electrospinning. This study presents a facile method for incorporating AgPs into the fiber mat by *in situ* reduction of silver nitrate by the electrospinning solvent, 2:1 acetone/N,N Dimethyl acetamide (DMAc). The solution of CA/PEG/AgPs was electrospun and the obtained fiber mat was characterized by field emission scanning electron microscopy (FESEM) which revealed smooth fibers of CA with a diameter in the range 250–400 nm. Interestingly, the surface of the fibers appeared striated on addition of the PEG. FESEM also showed AgPs of size 10 nm incorporated into the fiber. Formation of AgPs was also confirmed by UV–Vis, which generated Plasmon peak at 420 nm. It appeared that PEG not only stabilized the formed AgPs against agglomeration but also improved water uptake of the CA fiber mat by ~ 95%. This improved swelling property of the fiber mat shows the ability to absorb more wound exudates. Attenuated total reflectance-Fourier transform infrared spectroscopy (ATR-FTIR), differential scanning calorimetry (DSC), X-ray diffraction (XRD) and tensile test were performed to analyze the structural, thermal and mechanical properties of the CA/PEG/AgPs fiber mat. Finally, the electrospun fiber mat showed satisfactory antibacterial efficacy against gram-negative bacteria *Escherichia coli* (*E. coli*) and gram-positive bacteria *Staphylococcus aureus* (*S. aureus*).

**Keywords** Electrospinning · Cellulose acetate · Silver particles · Polyethylene glycol · Antibacterial effect · *In situ* reduction

## Introduction

Electrospinning has been acknowledged as a versatile and the most reported approach for electrostatic fabrication of polymeric fibers with diameters ranging from tens of nanometer to micrometer under the influence of a high voltage [1, 2]. This range of fiber size is highly beneficial as this possesses high surface area, substantial permeability, structural uniqueness and functionality which render their use in multifaceted applications such as wound dressing applications, tissue engineering, drug delivery, filtration, heavy metal adsorptions etc. [3, 4]. Among the various tested polymers for electrospinning, cellulose acetate (CA) stands out as the consummate choice of polymer in this study by virtue of its biocompatibility, significant biodegradability, hydrophilicity and overall moisture management capacity [5]. Distinctly, in antibacterial applications, the aforementioned properties of CA make it a suitable and desirable biopolymer and presents a myriad of scope to explore beyond the established works of CA [6].

In order to fabricate functional CA fibers with antibacterial properties and therefore, as a potential wound dressing material, silver particles (AgPs) have been produced *in situ* in the polymer solution and electrospun subsequently in this work. This *in situ* chemical reduction of silver nitrate ($AgNO_3$) provides a facile and nontoxic way to produce AgPs by eliminating the high power cost, labor of separating large volumes of organic solvents and oil bath from the final product associated with other

✉ M Tarik Arafat
tarikarafat@bme.buet.ac.bd

[1] Department of Materials and Metallurgical Engineering, Bangladesh University of Engineering and Technology (BUET), Dhaka 1000, Bangladesh

[2] Department of Glass and Ceramic Engineering, Bangladesh University of Engineering and Technology (BUET), Dhaka 1000, Bangladesh

[3] Department of Biomedical Engineering, Bangladesh University of Engineering and Technology (BUET), Dhaka 1205, Bangladesh

reduction methods such as physical methods, micro-emulsion method, microwave-assisted synthesis etc. Also, it provides a one-step fabrication route compared to the *ex situ* methods and hence minimizes the fabrication steps. In addition, chemical *in situ* reduction of $AgNO_3$ to AgPs in CA/PEG solution offers more uniform distribution of particles in the polymer matrix and also allows greater control over particle size [7]. These AgPs have been well-established in the field for the past two decades, and their potency as antibacterial agents has been well-documented in the literature [8]. However, there is much less attraction between inorganic particles and polymeric materials due to difference in their surface energies that causes repellency [9, 10]. Thus, these AgPs require stabilization that prevent them from getting agglomerated which can otherwise plummet their antibacterial activity [11]. Moreover, the fibers should also retain optimal swelling properties in order to provide a moist wound healing environment. Fibers with adequate swelling are able to absorb more of the wound exudates without being firmly adhered to the site. As a result, it will alleviate the pain of removing wound dressing patches, which dry out readily. This adhesion problem can be prevented by a high water content material, which in turn stimulates tissue regeneration process [12–14].

To meet these criteria, PEG of molecular weight 200 g/mol and 6000 g/mol (PEG 200 and PEG 6000) have been exploited in this work. The purpose of using a low and a high molecular weight of PEG (i.e. PEG 200 and PEG 6000) was to evaluate their effect on electrospinning of CA, due to contrasting physical states, and its corresponding fiber properties. PEG offers desirable features such as hydrophilicity, flexibility and nontoxicity required for bio-based applications. It has also been reported to play a role in modifying surface properties of fibers to have a better grip in the contact layer of the wound sites [15]. Additionally, there is good affinity and bonding between the epidermal growth factor (EGF) and PEG which can be intended towards the wound site [16]. However, swelling behavior of electrospun CA/PEG fibers has not been widely analyzed in literature. The role of PEG on swelling has also been investigated in this study due to some recent reports on it to improve swellability. In a recent study, PEG has been combined with poly-ε-caprolactone (PCL) to enhance the hydrophilicity. It was observed in the study that with increasing PEG content, water uptake increased due to the swelling of the PEG chain in the fiber mat and this was claimed to absorb more wound exudates [17]. Furthermore, the functioning of PEG as a stabilizer is also well-documented in literature [18, 19]. PEG stabilizes the AgPs which tend to compress and neutralize with aggregation due to van der Waals forces [20, 21]. Stabilization of these AgPs is induced by the short-range repulsive hydration forces of the hydrophilic PEG [22, 23].

Previously, CA/PEG fiber was fabricated with a view to establish PEG as a phase change material (PCM) where PEG was directly electrosprayed on separately electrospun CA fiber mat [24]. Also, CA was electrospun with PEG of molecular weight 10,000 for thermal energy storage applications [25]. The role of CA has been investigated dynamically as in fabricating core–shell nanostructure for drug delivery by Yang *et al.* [26], loading gallic-acid for wound dressing products by Wuttich-aroenmongkol *et al*. [27], and incorporating propolis into the CA fiber for producing water-repellent mats by Khoshnevisan *et al*. [28]. Recently, electrospun CA, CA/iron oxide nanoparticles fibers have drawn extensive attention for the fabrication of water purification membrane, magnetic hyperthermia and drug delivery applications [29–32]. Furthermore, antibacterial wound dressing synthesis using AgPs has gone a long way too. Abdel-Mohsen and his group electrospun polyvinyl alcohol/hyaluronan with *in situ* reduced Ag nanoparticles (AgNPs) where hyaluronan acted as the reducing and capping agent for AgNPs [33]. Wang *et al*. introduced a novel nanofibrous mat for wound dressing composed of polyurethane/keratin/AgNPs, where AgNPs were immobilized on the fiber surface by immersion technique [34]. Uttarayat and his team reported silk fibroin electrospun fiber mat coated with AgNPs for wound dressings. They utilized gamma irradiation method to produce AgNPs with a size of ~ 24 nm in the fiber [35]. Electrospun chitosan nanofibers with AgNPs were reported by Lee *et al.* with good antibacterial activity [36]. Also, multicomponent nanofibrous mat, chitosan/AgNPs/Polyvinyl alcohol, was reported by Abdelrahman *et al.* where AgNPs (25 nm diameter) were capped by chitosan and reduced by glucose [37]. However, to our knowledge electrospinning a nanofibrous mat by blending a solution of CA and PEG with *in situ* reduced AgPs has not been studied earlier with a purpose to evaluate the role of PEG in benefitting wound dressing and study the efficacy of the reduced AgPs in CA fiber matrix in preventing bacterial growth.

Thus, this study aimed at the electrospinning of CA/PEG/AgPs non-woven fiber mat, where AgPs have been reduced *in situ* via a chemical reaction with the electrospinning solvent itself and stabilized by the PEG. Furthermore, this work studied the influential role of PEG in incrementing the swelling property of the CA/PEG/AgPs fiber mat and analyzed the effect of PEG concentration on electrospinning behavior of CA fiber. Hence, this work is targeted towards bringing a novel composition of electrospun fiber mat, CA/PEG/AgPs, with improved functional and antibacterial properties.

## Materials and methods

### Materials

Cellulose acetate (CA) of molecular weight 30 kDa and silver nitrate ($AgNO_3$) from Sigma Aldrich were obtained. The

solvents- acetone and N,N-dimethylacetamide (DMAc), and the stabilizer- polyethylene glycol (PEG) of molecular weight 200 and 6000 were procured from Merck. Mannitol Salt Agar Base and EMB Agar Base were purchased from Himedia, India. All the chemicals were used without further purification.

## Preparation of solutions and electrospinning of nanofibrous mat

Electrospinning was performed based on our previous experiment using an in-house electrospinning setup [38, 39]. In brief, 17 wt% CA was found to dissolve and electrospun in 2:1 acetone/DMAc without any beads in the fiber. From our previous study, the voltage, feed rate and needle tip to collector distance were fixed at 20 kV, 1.5 ml/h and 10 cm respectively [39]. The above solution was further stirred with 5, 10, 20, 40 and 80 wt% PEG-200 and 2 and 5 wt% PEG-6000 of CA. Higher percentages of PEG-6000 was avoided as the CA solution turned too viscous to electrospin. After obtaining homogeneous and clear solution, it was electrospun for 2 h to obtain sufficient deposit of fiber mat. After electrospinning, the fiber mat was deposited on the collector which was then dried overnight at room temperature for further characterizations. In the later sections, the term 'solvent' has been referred to 2:1 acetone/DMAc all along the study.

## *In situ* reduction of $AgNO_3$ to *AgPs*

The electrospun fiber with AgPs was achieved when the CA/PEG solution was treated with 1 wt% $AgNO_3$ with respect to the weight of CA and subsequently reduced *in situ* via the electrospinning solvent. On adding $AgNO_3$ in the solution and stirring for 3 h, the transparent color of the CA/PEG solution started to turn slightly yellowish which gradually darkened to reddish brown with time. The mechanism of the reduction process has been discussed in the later part of this study. The concentration of $AgNO_3$ has been maintained constant (1 wt%) for better analyses of the effect of PEG on the stabilization of the AgPs and their antibacterial activity against the bacteria.

## Nanofibers characterization

### FESEM analysis

Geometric features such as fiber morphology and fiber diameter were characterized using FESEM (JEOL JSM 7600F, Tokyo, Japan) at an accelerating voltage of 5 kV. The CA fibers were sputter coated with gold before imaging. EDX was performed to determine the elemental composition of silver loaded fibers along with FESEM. The fiber diameters were determined by measuring at least 100 individual fibers with the ImageJ software.

### UV–visible spectroscopy

UV–visible spectroscopy of the CA/PEG solutions with AgPs was recorded on a UV-3100 spectrophotometer JP Selecta (Barcelona, Spain) with disposable polystyrene cuvettes to ascertain the formation of AgPs.

### XRD analysis

The structural parameters of the CA/PEG/AgPs fiber mat were investigated by X-ray diffractometer (3040-X'Pert PRO, Netherlands) from 5° to 80° at 2θ position with scanning speed of 2° $min^{-1}$ at room temperature. The X-ray powder diffraction technique was practiced with a primary beam power of 40 kV and 40 mA for CuKα (λ = 1.54056 Å) radiations.

### ATR-FTIR

Chemical and structural analysis were investigated by ATR-FTIR (Thermo Fisher Nicolet iS5, Ohio, USA) spectra. Scanning was conducted from 4000 to 650 $cm^{-1}$ with a resolution of 4 $cm^{-1}$ and a scanning interval of 2 $cm^{-1}$ with 64 repetitious scans averaged per sample.

### Tensile Test

Mechanical properties were analyzed using tensile tests. The tensile tests were performed on electrospun fiber mats with Shenzhen Wance Testing machine (China) using a load cell 10 N. The samples were of 5 mm x 30 mm × 0.25 µm. A preload of 0.001 N was applied and a strain rate of 2 mm/min and a gauge length of 20 mm were used.

### DSC analysis

Thermal behavior of CA fibers was evaluated using DSC (Shimadzu, DSC-60, Japan) where, the samples were heated up to 250 °C. Approximately, 15 mg unmodified CA fiber mat, modified CA/PEG and CA/PEG/AgPs were analyzed in an aluminum-pan under the nitrogen atmosphere at the heating rate of 10 °C/min.

### Swelling measurements

CA, CA/PEG, CA/AgPs and CA/PEG/AgPs fiber mats were cut into 1 × 1 $cm^2$ and dried in an oven at 40 °C overnight to determine their dry weight ($W_d$). The dried fiber mats were then soaked in deionized water for 1 h and 24 h separately.

The swollen fibers were removed from water, blotted of excess fluid with filter paper, and weighed to get the wet weight ($W_t$). The water uptake was calculated from the following formula:

$$\text{Water uptake } (\%) = [(W_t - W_d)/W_d] \times 100 \quad (1)$$

### Antibacterial evaluation

The antibacterial activity of the mats were quantitatively evaluated using the colony forming unit (CFU), because adsorption and inhibition of bacterial cell properties are more appropriate. The bacteria used in this study were *E. coli* (strain 231-b) and *S. aureus* (strain RM_AST_SA012) as model organisms. *S. aureus* was isolated from the throat and *E. coli* from local pond water [40]. The isolation process of the bacteria and strain number identification has been described in detail in the Online Resource (A, B, Fig. S1). The bacterial colonies were extracted with a loop and transferred to the sterilized nutrient broth. The broth is incubated at 35–37 °C for 24 h. Afterwards, culture in the broth solution was diluted with 0.85% saline to the concentration $4.0–5.0 \times 10^8$ CFU/ml. Saline was used to dilute since it prevents bacterial lysis due to osmotic pressure and also inhibits their growth and keeps the bacteria count steady. To test for blank control, 100 µL diluent was then spread on the nutrient agar plates and incubated. The electrospun fiber mats were then introduced into the $4.0–5.0 \times 10^8$ CFU/ml diluted broth solutions containing *E. coli* and *S. aureus* separately. After incubating, 100 µL of this culture solution containing samples were spread on agar plates. All the plates were incubated at 37 °C for 24 h prior to enumeration. The percentage of mortality of each bacterium was calculated with the following equation:

$$\text{Mortality } (\%) = [(A - B)/A] \times 100 \quad (2)$$

Where, A and B are the number of viable bacterial colony forming units (CFUs) recovered from the blank control and treated sample specimen after specified time interval, respectively.

## Results

### Morphological Analysis

FESEM revealed the bulk morphology of the electrospun CA, CA/PEG and CA/PEG/AgPs fiber mats in Fig. 1. CA yielded smooth, uniform fibers with diameters ranging from 250–400 nm as in Fig. 1a.

Upon incorporating PEG 200 (5, 10, 20, 40 and 80 wt% of CA) into the CA solution, uniformity was slightly altered. PEG 200 of concentration 5, 10 and 20 wt% did not affect the homogeneous distribution of the fibers as shown in

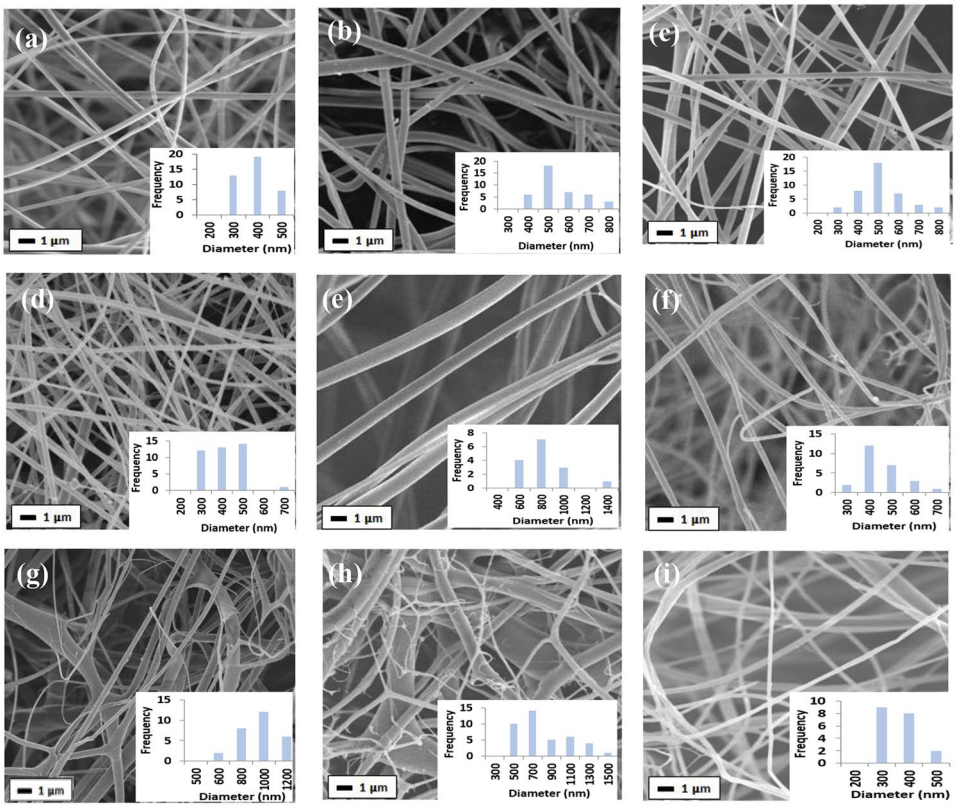


**Fig. 1** FESEM (5000X) of fibers electrospun in (**a**) CA-solvent. FESEM of CA-solvent with the following concentrations of PEG 200 (**b**) 5 wt% (**c**) 10 wt% (**d**) 20 wt% (**e**) 40 wt% and (**f**) 80 wt%. FESEM of CA-solvent with the following concentration of PEG 6000 (**g**) 2 wt% (**h**) 5 wt%. FESEM of (**i**) CA-solvent and 10 wt% PEG 200 with 1 wt% $AgNO_3$. The inset showed the fiber diameters in nanometer scale

Fig. 1b, 1c and 1d. However, with increasing concentration to 40 and 80 wt% non-uniformity was observed. As can be seen in Fig. 1e and 1f, fiber strands appeared fused with visible irregularities. These irregularities increased when fibers with PEG 6000 (2 and 5 wt% of CA) were electrospun as indicated in Fig. 1g and 1h along with the magnified images provided in the Online Resource (Fig. S2).

Also, electrospinning with high molecular weight of PEG i.e. PEG 6000 was inconvenient as inadequate amounts of fiber mat got deposited. Due to higher molecular weight of PEG, the CA solution turned quite viscous by the greater macromolecule chain entanglement which suppressed the elasticity and hindered the flow of solution [41]. On the other hand, the fiber diameters were reduced when electrospun with PEG 200 as compared to PEG 6000. This can be attributed to the fact that there is comparatively less polymer–solvent interaction between PEG 200 and 2:1 acetone/DMAc mixture due to shorter chain length of PEG 200 as compared to PEG 6000. As can be seen from the solubility parameters in Table 1, there is much greater difference between the Hansen's three dimensional solubility parameter ($\delta_t$) of PEG 200 and the solvent than that of PEG 6000 and the solvent. Higher miscibility and chain entanglement is anticipated when $\delta_t$ of different materials are similar.

Thus PEG 200 did not initiate strong macromolecular chain entanglement due to more difference in $\delta_t$, with CA solution resulting in lower but sufficient viscosity which rendered electrospinning smooth and uniform and in such cases segments of polymer chain tend to attract each other that might have caused shrinkage of polymer chain and consequently the fiber diameters decreased [42]. Also, this is consistent with the fact that lower viscosity causes decrease in fiber diameter as reported earlier [43].

Thus, PEG 6000 was not explored here for further modifications due to its difficulty in spinning and irregular morphology. Although different concentration of PEG 200 with CA-solvent was electrospun in the former part of this study, 10wt% was selected to be suitable for functionalizing with $AgNO_3$ based on morphology and AgPs distribution on the fiber surface. Figure 1i showed the bulk morphology of CA fiber with 10 wt% PEG 200 and 1 wt% $AgNO_3$. Higher concentration of PEG was reported to induce non-uniformity in fiber [24]. That is why, 10wt% appeared optimum concentration here. Thus, 10 wt% PEG 200, simply referred as PEG henceforth, was selected for the subsequent experiment without the likelihood of generating unfavourable fiber morphology.

**Table 1** Hansen solubility parameters for different materials [44]

| Chemicals | $\delta_t$ at 25°C $(MPa)^{1/2}$ |
|---|---|
| Acetone | 19.93 |
| DMAc | 22.77 |
| 2:1 acetone/DMAc | 20.87[a] |
| PEG 200 | 26.1 |
| PEG 6000 | 22.4 |
| Cellulose acetate | 19.89 |

[a]Calculated from $\delta_t = \sum \phi_i \delta_i$, where $\phi_i$ is the volume fraction and $\delta_i$ is the Hildebrand parameter

Figure 2 showed the magnified images of the CA, CA/PEG and CA/PEG/AgPs to compare the morphological changes associated with the addition of PEG and $AgNO_3$. The smooth CA fibers in Fig. 2a developed surface striations in the longitudinal directions on adding PEG in the Fig. 2b. These striations were supposed to appear due to limited compatibility between the bulk CA and the hydrophilic PEG that caused partial PEG phase separation towards the fiber surface and formed loose fiber strands. This can be attributed to the difference in surface energies of the interacting chemical species [45]. In addition, the diffusivity rate of PEG was much slower than acetone/DMAc and thus PEG in the solvent took more time to accumulate and adsorbed on the surface forming striated layer [46]. This topographical striated texture of electrospun CA fiber has an advantage for cell adhesion, growth and proliferation [47]. The surface striations of the fiber mats allowed more air to be trapped between the interfaces than that of smooth fibers. This is expected to facilitate the permeation of oxygen and nutrients between the wound and the external surrounding [48, 49].

In later modification of the CA fiber to impart antibacterial agents into it, $AgNO_3$ was added to CA/PEG solution.

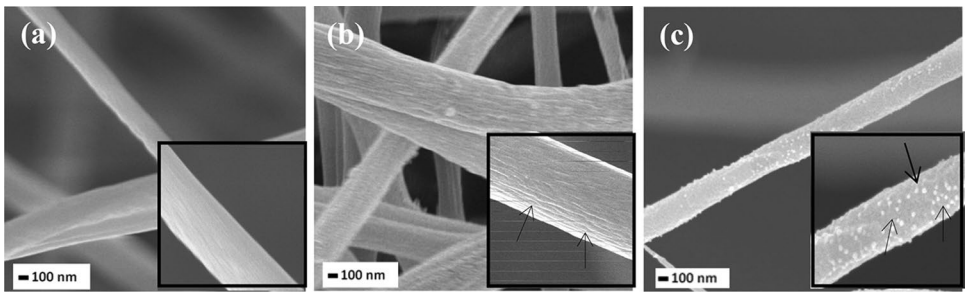


**Fig. 2** FESEM images (30000X) to compare morphological changes in (**a**) CA (**b**) CA/PEG and (**c**) CA/PEG/AgPs fiber. Inset shows magnified (100000X) images with arrows indicating surface striations and AgPs

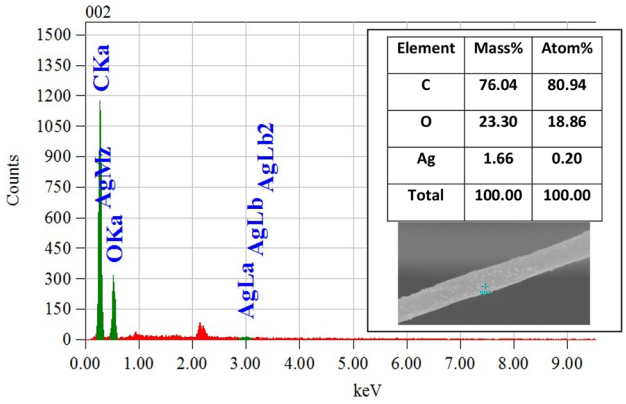


**Fig. 3** EDX spectra of CA/PEG/AgPs fiber

$AgNO_3$ was reduced in situ to AgPs and appeared on the fiber as shown in Fig. 2c. The particle size was determined to be ~ 10 nm which is coherent with earlier reported work [21]. The distribution of in situ reduced AgPs in Fig. 2c can be attributed to the stabilizing role of PEG. EDX analysis in Fig. 3 represented the elemental composition of the fiber and indicated the presence of trace amount of silver at 3.00 keV which is the typical optical absorption band peak of metallic Ag nanocrystallites due to surface plasmon resonance [50, 51].

## UV–Vis Analysis

To further ascertain the formation of AgPs UV–Vis spectroscopy was performed. The UV–visible spectrum of CA/PEG/AgPs solution, the dark brown solution with AgPs has been shown in Fig. 4.

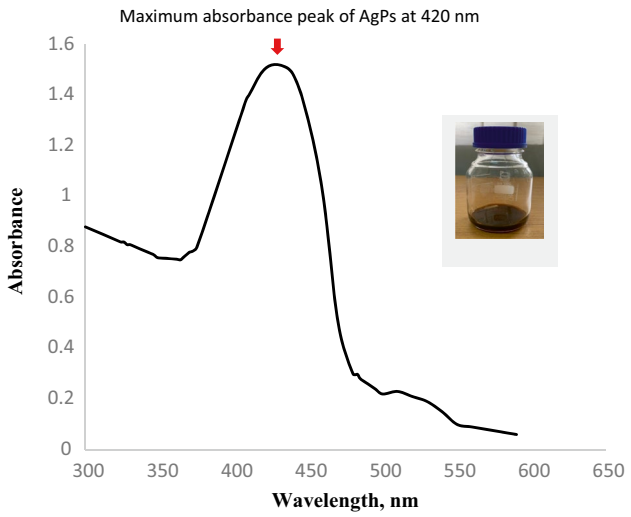


**Fig. 4** UV–vis spectrum of CA/PEG/AgPs solution containing 1 wt% $AgNO_3$

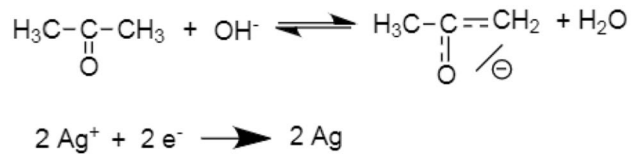


**Scheme 1** Reduction mechanism of $Ag^+$ to $Ag^0$ by the action of acetone/DMAc

The maximum absorbance at 420 nm in the spectrum was associated with the plasmon peak which corresponded to the surface- bound Ag particles [52, 53]. The spectral position of plasmon band absorption as well as its width was determined by the size and shape of the AgPs [54]. Thus, AgPs were formed *in situ* by the action of acetone/DMAc. The reduction occurred by the formation of $Ag^+$ ions which were reduced by the electrons donated from the acetone/DMAc to form $Ag^0$ atoms. Later, these atoms cluster together to form AgPs. The probable reaction mechanism for chemical reduction can be explained in the according to the scheme 1. The $OH^-$ from CA stripped a proton from an acetone molecule forming a carbanion ion which then rapidly reacted with another carbanion ion available in the solution due to the presence of acetone/DMAc and released the electron necessary for $Ag^+$ reduction to $Ag^0$ [55].

## XRD Analysis

The XRD diffractogram of CA/PEG/AgPs fiber mat was illustrated in Fig. 5.

The semi-crystalline nature of cellulose acetate was evident from the two peaks at 9.50° and 13.13°. PEG also

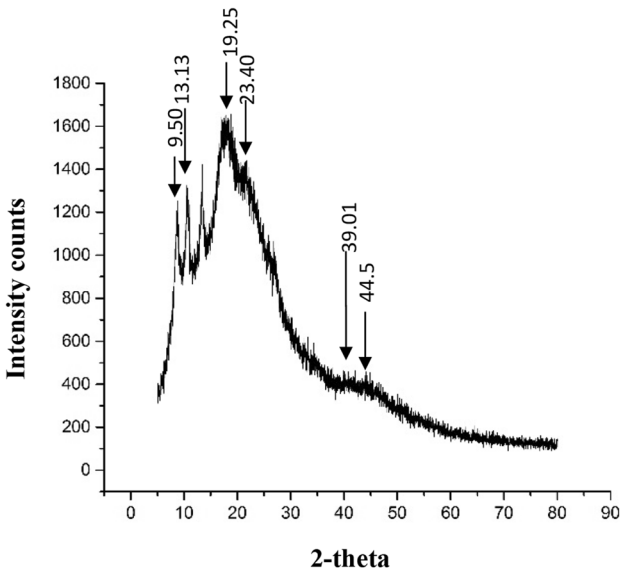


**Fig. 5** XRD diffractogram of CA/PEG/AgPs fiber mat

showed its characteristic peak at 19.25° and 23.40° [56]. The characteristic peak of AgPs was detected at 39.01° and 44.5° corresponding to the (111) and (200) planes respectively. These two peaks corresponded to the face-centered cubic (fcc) structure (rutile and anatase) of the metallic AgPs. The peak at 39.01° is not strong as reported in earlier literature [57–60]. This might be attributed to the reduction mechanism of acetone/DMAc. Due to their reduction mechanism the peak at 44.5° appeared more prominent. Other characteristic peaks of AgPs were less prominent here due to the lower percentage of $AgNO_3$.

The full width at half-maximum (FWHM) of the strongest characteristic peak (200) is used to estimate the average crystallite size by applying the Debye–Scherrer equation: $D = K\lambda / \beta\cos\theta$. Here X-ray wavelength λ is 1.54056, K is the shape factor which is often assigned a value of 0.89, D is the average diameter of the crystals in angstroms, θ is the Bragg angle in degrees, and β is the full width at half-maximum of the strongest characteristic peak in radians. The result shows that the average silver particle size in the CA/PEG fibers is approximately 11.2 nm which is close to the size observed through FESEM [61].

## ATR-FTIR Analysis

Molecular structure of CA and structural changes, if any, associated with the addition of PEG and $AgNO_3$ to CA are analyzed with ATR-FTIR. The obtained spectrum of CA, PEG, AgPs and CA/PEG/AgPs is shown in Fig. 6. In the case of pure CA, a broad peak at 3310 $cm^{-1}$ represented stretching of O–H bond, 2881 $cm^{-1}$ displayed the stretching of C-H bond, an intense peak at 1736 $cm^{-1}$ depicted the vibration of the acetate group, C = O. Symmetric and antisymmetric bending of methylene groups were observed at 1239 and 1053 $cm^{-1}$.

Besides, PEG showed its characteristic peak at 1100 $cm^{-1}$ and 1346 $cm^{-1}$ which indicated the crystalline phase of PEG. Also, C-H stretching of PEG was prominent at 2878 $cm^{-1}$ [62]. The spectrum of AgPs showed several peaks of which the peak at 3350 $cm^{-1}$ is broad and can be assigned to the stretching of hydroxyl groups due to the presence of alcohols and 2917 $cm^{-1}$ is for the C-H stretching. The sharp peak at 1384 $cm^{-1}$ and 1650 $cm^{-1}$ referred to the stretching of C-N and C = O present in DMAc [63]. The interactions of CA/PEG/AgPs fiber are confirmed by the FTIR spectra. The intensity of the peak at 3310 $cm^{-1}$ in CA appeared more prominent in CA/PEG/AgPs. This increased intensity occurred when the self-hydrogen bonded O–H groups in CA formed intermolecular hydrogen bonding with PEG. However, as appeared from the morphological analysis that there occurred partial phase separation of PEG, all the –OH end groups of PEG could not form intermolecular hydrogen bonding with oxygen atoms of cellulose acetate.

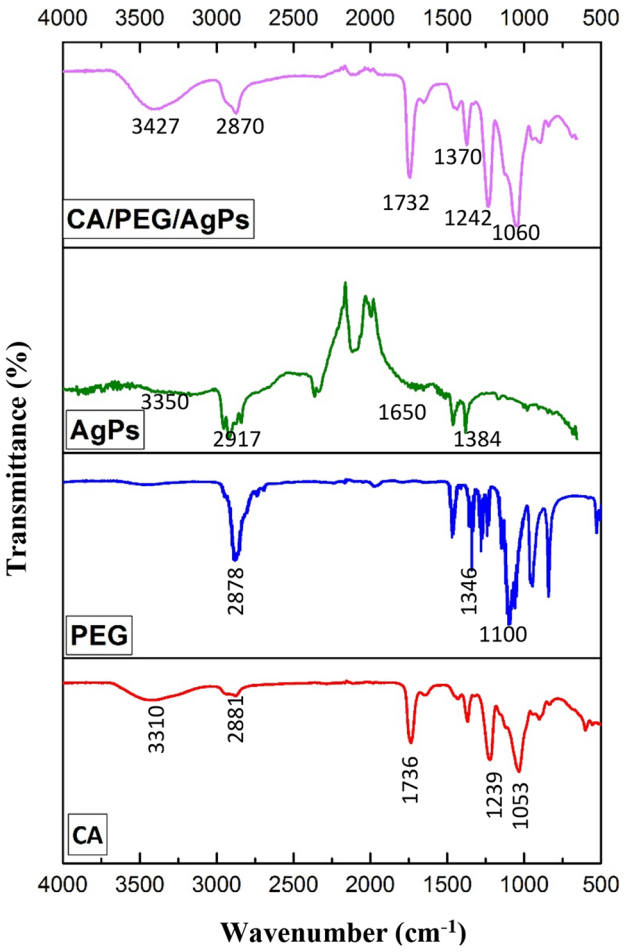


**Fig. 6** ATR/FTIR spectra of CA, PEG, AgPs and CA/PEG/AgPs fiber

Carbonyl peak was shifted from 1736 $cm^{-1}$ to 1732 $cm^{-1}$ in CA/PEG/AgPs fiber which was due to the interactions of the $OH^-$ group in PEG and the carbonyl group in CA. This weakening of carbonyl peak was also associated with the addition of Ag metal to the fiber. The shifting of C-O bond from 1239 $cm^{-1}$ to slightly higher frequency of 1242 $cm^{-1}$ was attributed to the binding of C = O and C-O with Ag particles [46, 64]. Also, electrostatic ion–dipole interaction was expected between CA and Ag. The acetate groups combined with oxygen were expected to react with Ag metal as shown in Fig. 7.

## Thermal Analysis

DSC was performed to observe the thermal changes associated with CA on adding PEG and AgPs. DSC thermograms in Fig. 8 displayed an endothermic event for CA located at around 50–110 °C which is attributed to the desorption of water.

Desorption occurs due to presence of residual moisture or low boiling point solvents and varies on the account

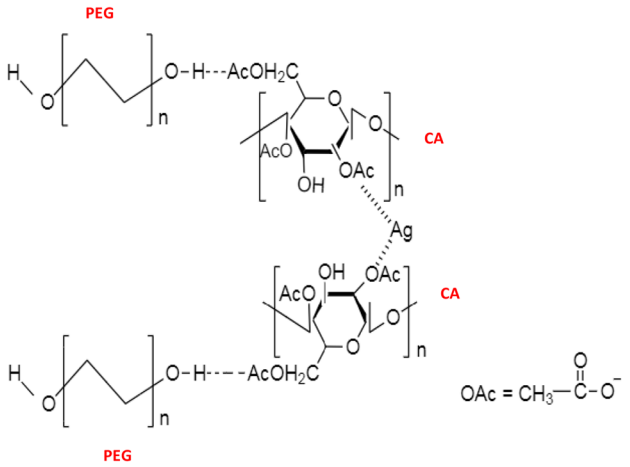


**Fig. 7** Electrostatic attraction between Ag and acetyl group of CA

of degree of substitution in CA [64]. The glass transition temperature, $T_g$, is located over a range of 120–150 °C for CA which was evident by the gradual shifting of the base upwards. An endothermic peak at 220–230 °C corresponded to the melting range of CA [65]. On the addition of PEG 200, the $T_g$ shifted to a lower temperature of 70–100 °C whereas no melting peak was observed within a temperature region of 250 °C. This degraded shift in $T_g$ can be interpreted as such that low molecular PEG, being hydrophilic in nature, interrupted the strong interactions of CA chains and increased the mobility by serving as an interchain lubricant, and finally resulted in lower $T_g$ [66–69]. This lowering of $T_g$, in turn, corroborated the FESEM analyses where it was explained that PEG had poor interaction with the CA solution and increased the chain flexibility which might have triggered partial phase separation of PEG towards the surface. A broad endothermic peak between 25–100 °C was observed for CA/PEG/AgPs fiber sample for desorption of water. Also, a sharp rise in base for this sample was also evident and corresponded to an increased $T_g$ of ~ 115 °C. This increase can be attributed to the interaction between the reduced AgPs with CA chain that restricted the chain mobility to some extent and caused an increase in $T_g$ [70].

## Swelling Behavior Analysis

The capacity of the fiber mat to retain body fluid, metabolites and wound exudates rapidly is another essential feature of wound dressing patches [71].

Figure 9 represented the swelling characteristics of CA fiber mats with and without PEG. As seen from the bar chart, the water content of CA fiber mat was around 350% after 24 h immersion. With the presence of 10% PEG of CA, the ability to retain water increased to 680% which is remarkably higher than the previous value. This was also valid when only CA/AgPs mat was tested for swelling. The water uptake escalated in presence of PEG with CA/AgPs. This phenomenon was attributed to the presence of a hydrophilic ethylene glycol unit of PEG performed as hydrogen bond donors/acceptors and could combine with water molecules [72]. PEG was evaluated for swelling improvement in case of PEG/tartaric acid crosslinked chitosan hydrogel film where the maximum attainable swelling was found to be around 353% [73]. Thus, PEG rendered fiber more swellable

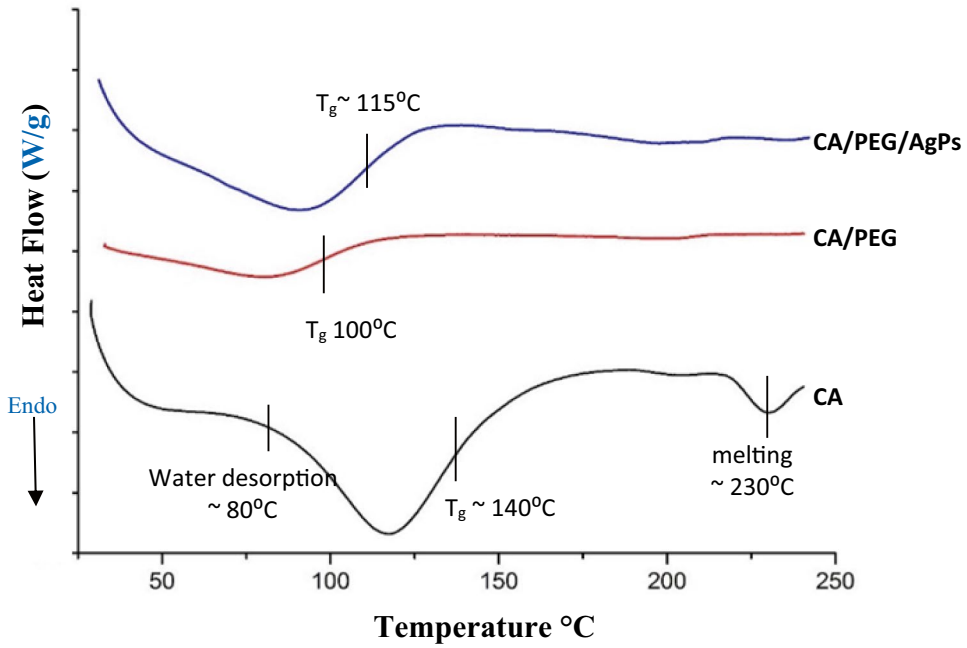


**Fig. 8** DSC thermogram of CA, CA/PEG and CA/PEG/AgPs fiber mats

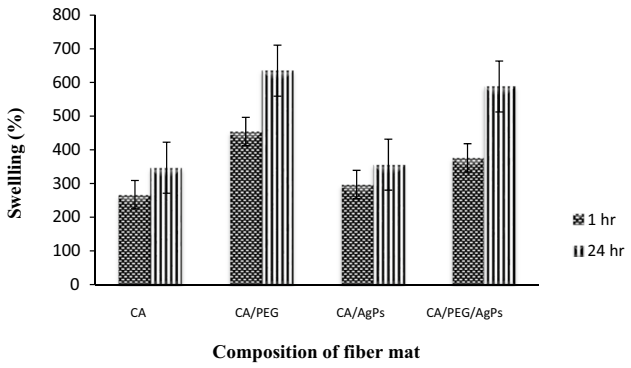


**Fig. 9** Water uptake of different fiber mats at 1 h and 24 h

in this study than that of film, which can be proved to have greater efficacy for, wound exudate absorption.

## Mechanical Property Analysis

The tensile strength and elongation were determined to estimate the mechanical properties of unmodified CA fiber mat and modified mat with PEG and AgPs.

Figure 10a showed the tensile stress for unmodified CA fiber, which was significantly lower with a value of 0.012 MPa. However, when modified with PEG, the stress increased to 0.033 MPa with a strain of 55% before failure. Also, the stress value was found to increase for CA/PEG/AgPs over CA/PEG fiber mat with a value of 0.044 MPa whereas, the strain value decreased to 10%. The elastic moduli, as shown in Fig. 10b also increased for modification with PEG and AgPs as compared to CA. With the grafting of Ag nanoparticles in CA fiber, the fiber could sustain higher load. Since, AgPs increased the strength here, it was assumed that the particle dispersion and chemical interactions between CA and AgPs were optimum. In earlier report, it was found that after exceeding a critical concentration, AgPs tend to agglomerate acting as the stress concentrator and thus reduce the strength [74]. However, as the stress value increased here after incorporating AgPs, it further testified the prevention of agglomeration due to the incorporation of PEG as shown in FESEM images.

## Antibacterial Assay

The antibacterial capacity of Ag-loaded CA/PEG fiber mat was explored through a viable colony counting method (CFU). As represented in Fig. 11, the initial antibacterial efficacies of the sample, after 1 h, against *E. coli* was found to be ~ 49%. Nevertheless, the sample succeeded in eliminating 97% colony of *E. coli* after 24 h. In case of *S. aureus*, the sample showed rapid bacterial killing and ended up in 100% mortality after 24 h. The abilities of the AgPs loaded CA/PEG fiber mat in inhibiting growth of both the bacteria types were shown in Fig. 12. To ensure that the bacterial colony growth inhibition was solely due to the presence of AgPs in the fiber, the test was also conducted for the samples CA and CA/PEG as shown in the Online Resource (Fig. S3), which demonstrated no bacterial killing even after 24 h. The antibacterial action of AgPs is due to the destruction of bacterial cell membranes by the metal ions when bonded to the –SH (thiol) group of the cellular enzymes. Thus, it reduced the enzymatic activity of the bacteria critically up to the death of the cell. Also, the AgPs interfere with the bacterial DNA and inhibit their multiplication [75]. As it can be deferred from Fig. 11, the antibacterial action against *E. coli* was somewhat lower than that of *S. aureus* which is in agreement with previous studies [76]. This can be attributed to the different nature of cell walls between Gram-positive and Gram-negative bacteria. The cell wall of *E. coli* consists of lipids, proteins and

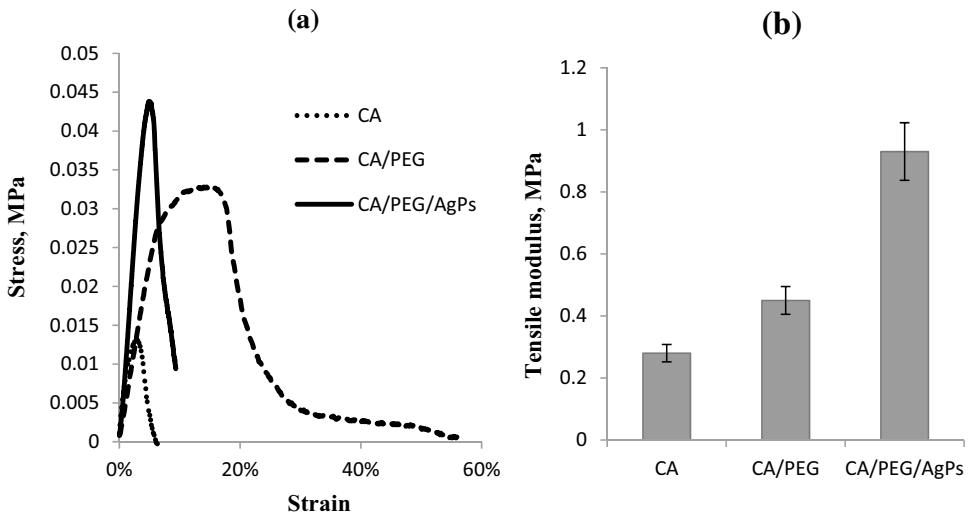


**Fig. 10** (**a**) Stress vs strain and (**b**) Tensile modulus plot for CA, CA/PEG and CA/PEG/AgPs fiber mats

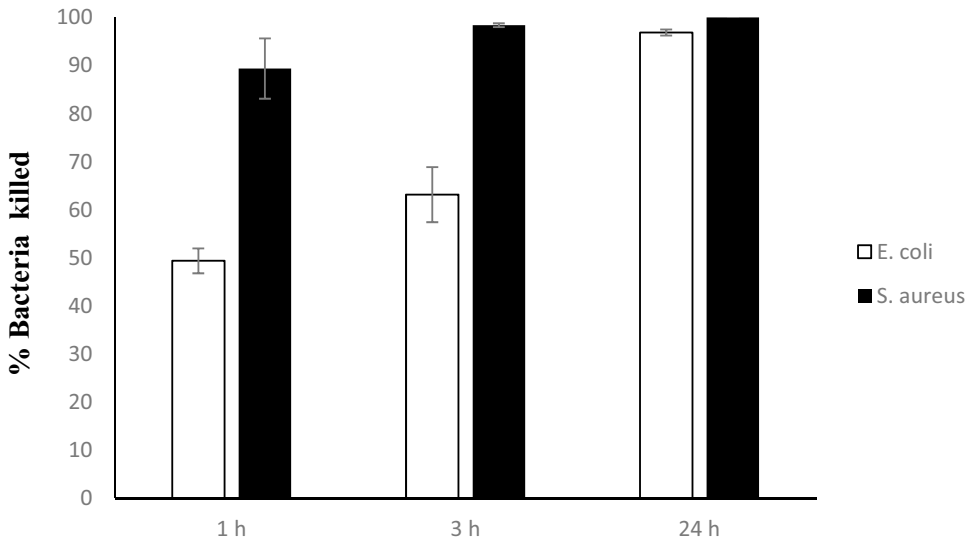


**Fig. 11** Bacteria killing rate at different time intervals

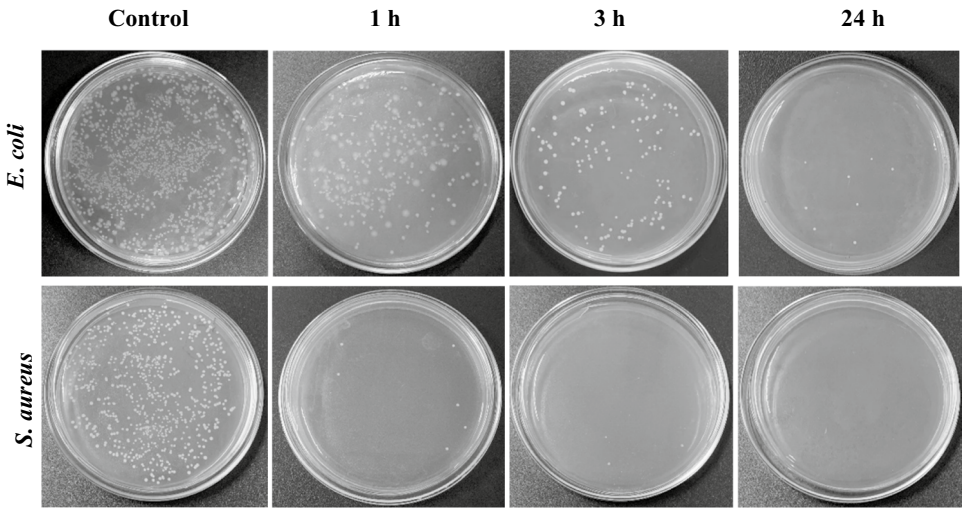


**Fig. 12** Antibacterial activity of the CA/PEG/AgPs fiber mat against *E. coli* and *S. aureus*

lipopolysaccharides (LPS) which provides a barrier against biocides whereas, the cell wall of Gram-positive bacteria, such as *S. aureus* does not consist of LPS and are more sensitive to the antibacterial action of AgPs.

Since Ag has higher affinity for sulfur and phosphorus in the cell membrane, the elements can readily react with each other in *S. aureus* as compared to *E. coli* due to the presence of LPS and form proteins that are baneful for the bacterial survival [77, 78]. Also, in case of this study, as can be seen from the Fig. 12, the number of bacteria colony is higher in the *E. coli* control than that of *S. aureus* which can contribute to the lesser efficacy of the fabricated CA/PEG/AgPs fiber mat against *E.coli* at identical time period observation.

## Conclusion

In this investigation, electrospinning was carried out using a solution consisting of CA, PEG and AgPs with a view to fabricate antibacterial fiber mat. AgPs were synthesized *in situ* by a chemical route where the solvent 2:1 acetone/DMAc acted as the reducing agent. The AgPs observed from FESEM measured 10 nm size, UV–vis spectra showing characteristic peak at 420 nm and EDS confirmed the presence of Ag. The role of PEG as a stabilizer of AgPs and a surface modifier was established as PEG prevented particle agglomeration at a concentration of 10 wt% and somewhat modified the fiber surface with striations without any further treatment of the fiber. These striations are expected

to improve cell attachment and aid the stabilization of the AgPs by eliminating the surface repellence otherwise observed for smooth fibers. Also, the fiber mat containing PEG showed increased swellability as high as twice as that of the fiber mat without PEG. This was indeed another enviable feature for wound dressing applications. The antibacterial efficacies of the produced fiber mat containing AgPs were successfully evaluated against *E. coli* and *S. aureus* at different time intervals where it showed complete elimination of *S. aureus* and nearly complete eradication of *E.coli*. Therefore, this antibacterial CA/PEG/AgPs fiber mat with improved swellability can have potential application in wound dressings.

**Supplementary Information** The online version contains supplementary material available at (https://doi.org/10.1007/s10965-020-02356-2).

**Acknowledgement** This project was funded by Bangladesh University of Engineering and Technology (BUET) under grant no: DAERS/CASR/R-01/2015/DR-2359(102).

## References

1. Rodríguez-Tobías H, Morales G, Grande D (2019) Comprehensive review on electrospinning techniques as versatile approaches toward antimicrobial biopolymeric composite fibers. Mater Sci Eng C 101:306–322
2. Ray SS, Chen SS, Nguyen NC, Nguyen HT (2018) Electrospinning: A Versatile Fabrication Technique for Nanofibrous Membranes for Use in Desalination. Nanoscale Mater Water Purif: 247–273
3. Kakoria A, Sinha-Ray S (2018) A Review on Biopolymer-Based Fibers via Electrospinning and Solution Blowing and Their Applications. Fibers 6:45
4. Haddad MY, Alharbi HF, Karim MR, Aijaz MO, Alharthi NH (2018) Preparation of $TiO_2$ incorporated polyacronitrile electrospun nanofibers for adsorption of heavy metal ions. J Polym Res 25:218
5. Kamal T, Ahmad I, Khan SB, Asiri AM (2017) Synthesis and catalytic properties of silver nanoparticles supported on porous cellulose acetate sheets and wet-spun fibers. Carbohydr Polym 157:294–302
6. Jatoi AW, Kim IS, Ni QQ (2019) Cellulose acetate nanofibers embedded with AgPs anchored $TiO_2$ nanoparticles for long term excellent antibacterial applications Carbohydr. Polym 207:640–649
7. Lu J, Moon K, Xu J, Wong CP (2006) Synthesis and dielectric properties of novel high- K polymer composites containing in-situ formed silver nanoparticles for embedded capacitor applications J Mater Chem 16:1543–1548
8. Zheng K, Setyawati MI, Leong DT, Xie J (2018) Antimicrobial silver nanomaterials. Coord Chem Rev 357:1–17
9. Cheng Q, Li C, Pavlinek V, Saha P, Wang H (2006) Surface-modified antibacterial $TiO_2$ / $Ag^+$ nanoparticles : Preparation and properties. Appl Surf Sci 252:4154–4160
10. Man XU (2008) Electrical properties of nano-silver / polyacrylamide / ethylene vinyl acetate composite. J Shanghai Univ 12:85–90
11. Černík M, Thekkae Padil VV (2013) Green synthesis of copper oxide nanoparticles using gum karaya as a biotemplate and their antibacterial application Int J Nanomedicine 889
12. Ngadaonye JI, Geever LM, Killion J, Higginbotham CL (2013) Development of novel chitosan-poly(N, N-diethylacrylamide) IPN films for potential wound dressing and biomedical applications. J Polym Res 20:161
13. Sung JH, Ma-R H, Kim JO, Lee JH, Kim YI, Kim JH, Chang SW, Jin SG, Kim JA, Lyoo WS, Han SS, Ku SK, Yong CS, Han-G C (2010) Gel characterisation and in vivo evaluation of minocycline-loaded wound dressing with enhanced wound healing using polyvinyl alcohol and chitosan. Int J Pharm 392:232–240
14. Murakami K, Aoki H, Nakamura S, Shin-ichiro N, Takikawa M, Hanzawa M, Kishimoto S, Hattori H, Tanaka Y, Kiyosawa T, Sato Y, Ishihara M (2010) Hydrogel blends of chitin/chitosan, fucoidan and alginate as healing-impaired wound dressings. Biomaterials 31:83–90
15. Gianino E, Miller C, Gilmore J (2018) Smart Wound Dressings for Diabetic Chronic Wounds. Bioeng 5:51
16. Mir M, Najabat M, Afifa A, Ayesha B, Munam G, Shizza A (2018) Synthetic polymeric biomaterials for wound healing : a review. Prog Biomater 7:1–21
17. He FL, Deng X, Zhou YQ, Zhang TD, Liu YL, Ye YJ, Yin DC (2019) Controlled release of antibiotics from poly-ε-caprolactone/polyethylene glycol wound dressing fabricated by direct-writing melt electrospinning. Polym Adv Technol 30:25–434
18. Liu Y, Wang Y, Zhao J (2019) Design, optimization and in vitro - in vivo evaluation of smart nanocaged carrier delivery of multifunctional PEG-chitosan stabilized silybin nanocrystals. Int J Biol Macromol 124:667–680
19. Anbarasu M, Anandan M, Chinnasamy E, Gopinath V, Balamurugan K (2015) Molecular and Biomolecular Spectroscopy Synthesis and characterization of polyethylene glycol ( PEG ) coated $Fe_3O_4$ nanoparticles by chemical co-precipitation method for biomedical applications. Acta Part A Mol Biomol Spectrosc 135:536–539
20. Fleitas-Salazar N, Silva-Campa E, Pedroso-Santana S, Tanori J, Pedroza-Montero MR, Riera R (2017) Effect of temperature on the synthesis of silver nanoparticles with polyethylene glycol: new insights into the reduction mechanism. J Nanoparticle Res 19:113
21. Díaz-Cruz C, Alonso Nuñez G, Espinoza-Gómez H, Flores-López LZ (2016) Effect of molecular weight of PEG or PVA as reducing-stabilizing agent in the green synthesis of silver-nanoparticles. Eur Polym J 83:265–277
22. Moore TL, Lorenzo LR, Hirsch V, Balog S, Urban D, Jud C, Rutishauser BR, Lattuada M, Fink AP (2015) Nanoparticle colloidal stability in cell culture media and impact on cellular interactions. Chem Soc Rev 44:6287–6305
23. Guerrini L, Alvarez-Puebla RA, Pazos-Perez N (2018) Surface modifications of nanoparticles for stability in biological fluids. Materials 11:1–28
24. Chen C, Wang L, Huang Y (2011) Electrospun phase change fibers based on polyethylene glycol / cellulose acetate blends. Appl Energy 88:3133–3139
25. Chen C, Wang L, Huang Y (2009) Crosslinking of the electrospun polyethylene glycol / cellulose acetate composite fibers as shape-stabilized phase change materials. Mater Lett 63:569–571
26. Yang Y, Li W, Yu DG, Wang G, Williams GR, Zhang Z (2019) Tunable drug release from nanofibers coated with blank cellulose acetate layers fabricated using tri-axial electrospinning. Carbohydr Polym 203:228–237
27. Wutticharoenmongkol P, Hannirojram P, Nuthong P (2019) Gallic acid-loaded electrospun cellulose acetate nanofibers as potential wound dressing materials. Polym Adv Technol 30:1135–1147

28. Khoshnevisan K, Hassan M, Hadi S, Shadab S, Sarrafzadeh MH, Larijani B, Dorkoosh FA, Haghpanah V, Khorramizadeh MR (2018) Cellulose acetate electrospun nanofibers for drug delivery systems: Applications and recent advances. Carbohydr Polym 198:131–141
29. Khoshnevisan K, Maleki H, Samadian H, Shahsavari S, Sarrafzadeh MH, Larijani B, Dorkoosh FA, Haghpanah V, Khorramizadeh MR (2018) Cellulose acetate electrospun nanofibers for drug delivery systems: Applications and recent advances. Carbohydr polym 198:131–141
30. Goetz LA, Naseri N, Nair SS, Karim Z, Mathew AP (2018) All cellulose electrospun water purification membranes nanotextured using cellulose nanocrystals. Cellulose 25:3011–3023
31. Matos RJR, Chaparro CIP, Silva JC, Almeida M, Paulo J, Soares PIP (2018) Electrospun composite cellulose acetate / iron oxide nanoparticles non- woven membranes for magnetic hyperthermia applications. Carbohydr Polym 198:9–16
32. Um-i-Zahra S, Shen XX, Li H, Zhu L (2014) Study of sustained release drug-loaded nanofibers of cellulose acetate and ethyl cellulose polymer blends prepared by electrospinning and their in-vitro drug release profiles. J Polym Res 21:602
33. Abdel-Mohsen AM, Pavliňák D, Čileková M, Lepcio P, Abdel-Rahman RM, Jančář J (2019) Electrospinning of hyaluronan/polyvinyl alcohol in presence of in-situ silver nanoparticles: Preparation and characterization. Int J Biol Macromol 139:730–739
34. Wang Y, Li P, Xiang P, Lu J, Yuan J, Shen J (2016) Electrospun polyurethane/keratin/AgNP biocomposite mats for biocompatible and antibacterial wound dressings. J Mater Chem B 4:635–648
35. Uttayarat P, Jetawattana S, Suwanmala P, Eamsiri J, Tangthong T, Pongpat S (2012) Antimicrobial electrospun silk fibroin mats with silver nanoparticles for wound dressing application. Fiber Polym 13:999–1006
36. Lee SJ, Heo DN, Moon JH, Ko WK, Lee JB, Bae MS, Park SW, Kim JE, Lee DH, Kim EC, Lee CH (2014) Electrospun chitosan nanofibers with controlled levels of silver nanoparticles. Preparation, characterization and antibacterial activity. Carbohydr Polym 111:530–537
37. Abdelgawad AM, Hudson SM, Rojas OJ (2014) Antimicrobial wound dressing nanofiber mats from multicomponent (chitosan/silver-NPs/polyvinyl alcohol) systems. Carbohydr Polym 100:166–178
38. Mahmud MM, Perveen A, Matin MA, Arafat MT (2018) Effects of binary solvent mixtures on the electrospinning behavior of poly (vinyl alcohol). Mater Res Express 5:115407
39. Majumder S, Matin MA, Sharif A, Arafat MT (2019) Understanding solubility, spinnability and electrospinning behaviour of cellulose acetate using different solvent systems. Bull Mater Sci 42:171
40. Mahmud M, Zaman S, Perveen A, Jahan RA, Islam F, Arafat MT (2019) Controlled release of curcumin from electrospun fiber mats with antibacterial activity. J Drug Deliv Sci Technol 55:101386
41. Chou WL, Yu DG, Yang MC, Jou CH (2007) Effect of molecular weight and concentration of PEG additives on morphology and permeation performance of cellulose acetate hollow fibers. Sep Purif Technol 57:209–219
42. Wongchitphimon S, Wang R, Jiraratananon R, Shi L, Heng C (2011) Effect of polyethylene glycol (PEG) as an additive on the fabrication of polyvinylidene fluoride- co -hexafluropropylene (PVDF-HFP) asymmetric microporous hollow fiber membranes. J Memb Sci 369:329–338
43. Nezarati RM, Eifert MB, Cosgriff-hernandez E (2013) Effects of Humidity and Solution Viscosity on Electrospun Fiber Morphology. Tissue Eng Part C 19:810–819
44. Lide DR (2003) CRC Handbook of Chemistry and Physics. CRC Press LLC, Boca Raton
45. Hendrick E, Frey M (2014) Increasing Surface Hydrophilicity in Poly (Lactic Acid) Electrospun Fibers by Addition of Pla-b-Peg Co-Polymers. J Eng Fiber Fabr 9
46. Li S, Jia N, Ma M, Zhang Z, Liu Q, Sun R (2011) Cellulose – silver nanocomposites : Microwave-assisted synthesis, characterization, their thermal stability, and antimicrobial property. Carbohydr Polym 86:441–447
47. Li Y, Xiao Y, Liu C (2016) The Horizon of Materiobiology : A Perspective on Material-Guided Cell Behaviors and Tissue Engineering. Chem Rev 117:4376–4421
48. Yu H, Chen X, Cai J, Ye D, Wu Y, Fan L, Liu P (2019) Novel porous three-dimensional nanofibrous scaffolds for accelerating wound healing. Chem Eng J 369:253–262
49. Cui W, Li X, Zhou S, Weng J (2008) Degradation patterns and surface wettability of electrospun fibrous mats. Polym Degrad Stab 93:731–738
50. Montazer M, Malekzadeh SB (2012) Electrospun antibacterial nylon nanofibers through in situ synthesis of nanosilver: preparation and characteristics. J Polym Res 10:9980
51. Duan YY, Jia J, Wang SH, Yan W, Jin L, Wang ZY (2007) Preparation of antimicrobial poly (ϵ-caprolactone) electrospun nanofibers containing silver-loaded zirconium phosphate nanoparticles. J Appl Polym 106:1208–1214
52. Smitha SL, Nissamudeen KM, Philip D, Gopchandran KG (2008) Studies on surface plasmon resonance and photoluminescence of silver nanoparticles. Acta Part A Mol Biomol Spectrosc 71:186–190
53. Ibrahim HM, El-Zairy EMR (2016) Carboxymethylchitosan nanofibers containing silver nanoparticles: Preparation, Characterization and Antibacterial activity. J Appl Pharm Sci 6:43–48
54. Zheng Y, Cai C, Zhang F, Monty J, Linhardt RJ, Simmons TJ (2016) Can natural fibers be a silver bullet? Antibacterial cellulose fibers through the covalent bonding of silver nanoparticles to electrospun fibers. Nanotechnology 27:055102
55. Halaciuga I, Laplante S, Goia DV (2011) Precipitation of dispersed silver particles using acetone as reducing agent. J Colloid Interface Sci 354:620–623
56. Trivedi MK, Nayak G, Patil S, Tallapragada RM, Mishra R (2015) Impact of Biofield Treatment on Chemical and Thermal Properties of Cellulose and Cellulose Acetate. J Bioeng Biomed Sci 5
57. Zheng J, Song F, Wang Y (2014) In-situ synthesis, characterization and antimicrobial activity of viscose fiber loaded with silver nanoparticles. Cellulose 21:3097–3105
58. Jeong SH, Yeo SY, Yi SC (2005) The effect of filler particle size on the antibacterial properties of compounded polymer / silver fibers. J Mater Sci 40:5407–5411
59. Mohseni M, Shamloo A, Aghababaie Z, Afjoul H, Abdi S (2019) A comparative study of wound dressings loaded with silver sulfadiazine and silver nanoparticles : In vitro and in vivo evaluation. Int J Pharm 564:350–358
60. Reza A, Kalantary H, Yousefi M, Ramazani A, Morsali A (2012) Synthesis and Characterization of Ag Nanoparticles @ Polyethylene fibers under Ultrasound irradiation. Ultrason Sonochem 19:853–857
61. Zhang Q, Wu D, Qi S, Wu Z, Yang X, Jin R (2007) Preparation of ultra-fine polyimide fibers containing silver nanoparticles via in situ technique. Mater Lett 61:4027–4030
62. Ghorani B, Russell SJ, Goswami P (2013) Controlled morphology and mechanical characterisation of electrospun cellulose acetate fibre webs. Int J Polym Sci 1–12
63. Amany A, El-Rab SFG, Gad F (2012) Effect of reducing and protecting agents on size of silver nanoparticles and their antibacterial activity. Der Pharma Chemica 4:53–65

64. Ahmad A, Jamshed F, Riaz T, Waheed S, Sabir A, AlAnezi AA, Adrees M, Jamil T (2016) Self-sterilized composite membranes of cellulose acetate / polyethylene glycol for water desalination. Carbohydr Polym 149:207–216
65. Tungprapa S, Jangchud I, Supaphol P (2007) Release characteristics of four model drugs from drug-loaded electrospun cellulose acetate fiber mats. Polymer 48:5030–5041
66. Sabitha M, Rajiv S (2015) Preparation and characterization of ampicillin-incorporated electrospun polyurethane scaffolds for wound healing and infection control. Polym Eng Sci 55:541–548
67. Capanema NSV, Mansur AAP, Jesus AC, Carvalho SM, Oliveira LC, Mansur HS (2018) Superabsorbent crosslinked carboxymethyl cellulose-PEG hydrogels for potential wound dressing applications. Int J Biol Macromol 106:1218–1234
68. Zhang C, Salick MR, Cordie TM, Ellingham T, Dan Y, Turng LS (2015) Incorporation of poly(ethylene glycol) grafted cellulose nanocrystals in poly(lactic acid) electrospun nanocomposite fibers as potential scaffolds for bone tissue engineering. Mater Sci Eng C 49:463–471
69. Zafar M, Ali M, Khan SM, Jamil T, Butt MTZ (2012) Effect of additives on the properties and performance of cellulose acetate derivative membranes in the separation of isopropanol/water mixtures. Desalination 285:359–365
70. Shi Q, Vitchuli N, Nowak J, Noar J, Caldwell JM, Breidt F, Bourham M, McCord M, Zhang X (2011) One-step synthesis of silver nanoparticle-filled nylon 6 nanofibers and their antibacterial properties. J Mater Chem 21:10330–10335
71. Shao W, Wu J, Wang S, Huang M, Liu X, Zhang R (2017) Construction of silver sulfadiazine loaded chitosan composite sponges as potential wound dressings. Carbohydr Polym 157:1963–1970
72. Xu Z, Li J, Zhou H, Jiang X, Yang C, Wang F (2016) Morphological and swelling behavior of cellulose. RSC Adv 6:43626–43633
73. Altinisik A, Yurdakoc K (2011) Synthesis, Characterization, and Enzymatic Degradation of Chitosan / PEG Hydrogel Films. J Appl Polym 122:1556–1563
74. Ghaffari T, Hamedi-rad F (2015) Effect of Silver Nano-particles on Tensile Strength of Acrylic Resins J Dent Res Dent Clin Dent. Prospects 9:40
75. Dastjerdi R, Montazer M, Shahsavan S (2009) A new method to stabilize nanoparticles on textile surfaces. Colloids Surf A Physicochem Eng Asp 345:202–210
76. Celebioglu A, Topuz F, Yildiz ZI, Uyar T (2019) One-step green synthesis of antibacterial silver nanoparticles embedded in electrospun cyclodextrin nanofibers. Carbohydr Polym 207:471–479
77. Guzman M, Dille J, Godet S (2012) Synthesis and antibacterial activity of silver nanoparticles against gram-positive and gram-negative bacteria. Nanomedicine Nanotechnology Biol Med 8:37–45
78. Xu X, Yang Q, Wang Y, Yu H, Chen X, Jing X (2006) Biodegradable electrospun poly(l-lactide) fibers containing antibacterial silver nanoparticles. Eur Polym J 42:2081–2087